

Communication

Stepwise Evolution of AgCl Microcrystals from Octahedron into Hexapod with Mace Pods and their Visible Light Photocatalytic Activity

Yuxiang Lu ^{1,2}, Yazhou Qin ¹, Dongdong Yu ³ and Jianguang Zhou ^{1,2,*}

¹ Research Center for Analytical Instrumentation, Institute of Cyber-Systems and Control, State Key Laboratory of Industrial Control Technology, Zhejiang University, Hangzhou 310027, China

² Department of Chemistry, Zhejiang University, Hangzhou 310027, China

³ Hospital of Zhejiang University, Zhejiang University, Hangzhou 310027, China

* Correspondence: jgzhou@zju.edu.cn

Received: 9 July 2019; Accepted: 1 August 2019; Published: 2 August 2019



Abstract: In this work, we have synthesized hexapods AgCl crystals with mace pods for the first time. Diallyldimethylammonium chloride (DDA)-controlled stepwise evolution of AgCl crystals from octahedron to hexapods with mace pods are achieved by one-pot method. The intermediates have been captured which show the basic process of crystal growth. In this process, octahedra AgCl crystals firstly grow along the $\langle 100 \rangle$ direction and then change to grow in the $\langle 110 \rangle$ direction. At the same time, the size of AgCl grow from 2 μm to 20 μm . Due to the poor absorption of visible light by AgCl, sodium borohydride (NaBH_4) is used to reduce AgCl hexapods with mace pods crystals. By changing the mole ratio (R) of NaBH_4 to AgCl, the new structure was reduced to obtain a series of Ag@AgCl microstructures. Visible light catalysis effects of the Ag@AgCl microstructures on degradation of methyl orange (MO) were investigated. The Ag@AgCl microstructures with $R = 0.02$ have a high photocatalytic performance, which completely degrades MO in 40 min.

Keywords: hexapod AgCl; one-pot method; Ag@AgCl microstructure; MO degradation

1. Introduction

Due to the vital role of micro/nanomaterials in the sustainable development of materials, the controllable preparation of micro/nanomaterials has attracted the interest of many researchers. In the past few decades, a great deal of research has been devoted to the morphology-controlled synthesis of metal crystals as their shape-dependent physical and chemical properties [1–5]. In particular, the shape controls the surface of metal micro/nanocrystals, such as the edge, steps, and corners, which controls their surface structure and catalytic active sites. So far, various shapes of novel metal micro/nanocrystals have been reported, such as spheres [6,7], cubes [8–10], plates [11–14], and rods [15–18]. More complex flower-like [19,20] and star-shaped [21] novel metal crystals have also been synthesized. Among different shapes of crystals, highly branched metal micro/nanostructures have been studied in depth owing to their high catalytic properties. For example, Yang et al. [22–24] reported that highly dendritic metal nanocrystals can be prepared by selective etching and anisotropic growth method. Xia and colleagues [25–27] reported that Pt and Pd crystals grew along the directions of $\langle 100 \rangle$ and $\langle 111 \rangle$ contain high-index facets including $\{520\}$, $\{830\}$, $\{730\}$ and $\{720\}$, which therefore exhibits exceptionally high electrocatalytic activity.

Among the many inorganic materials, silver halides, especially silver chloride (AgCl), have attracted the interest of many researchers due to their excellent photocatalytic properties. Since Hung et al. [28] reported that AgCl crystal is a plasma photocatalyst, it has been considered to be one of the most promising alternatives to conventional semiconductor photocatalysts. To date,

a large number of studies have shown that electronic transfer induced by surface plasmon resonance (SPR) results in high photocatalytic activity of AgCl [28–32]. Many kinds of methods such as ionic liquid-assisted hydrothermal, template directed and capping agent method have been used to fabricate well defined AgCl micro/nanocrystals, which includes nanospheres [33], nano cubes [34–36], caged cubes [37,38], plates [39,40] and nanowires [41–43]. Moreover, Lou and colleagues [44,45] synthesized concave cube AgCl microcrystals by a wet chemical oxidation approach. Using NaClO_2 to oxidize Ag plate to provide silver ions (Ag^+) and NaCl solution to provide chloride ion (Cl^-), high-index facets concave cube AgCl microcrystals with high catalytic activity was prepared at room temperature. By controlling the concentration of Ag^+ through oxidation, cube seed was preferentially grown along the directions of $\langle 111 \rangle$ and $\langle 110 \rangle$ in a high concentrated Cl^- solution forming the concave cube AgCl microcrystals. Furthermore, while under the condition of high concentration of NaCl, NaClO_4 , and citric acid, the cube seed was grown along the direction of $\langle 111 \rangle$ and eventually formed three-dimensional (3D) AgCl hierarchical superstructure. Furthermore, by the addition of Cl^- into a silver amine ($[\text{Ag}(\text{NH}_3)_2]^+$) complex, Gatemala et al. [46] prepared various highly branched 3D AgCl hierarchical microcrystals. Both of them found that highly branched 3D AgCl hierarchical microcrystals have excellent photocatalytic performance thanks to the high density of low-coordinated step atoms exposed on their surfaces. Therefore, in order to explore and realize the potential applications of new structure materials, there is still a need for efficient methods to precisely fabricate controlled complex micro/nanostructures.

In this work, the shape transformation of AgCl microcrystals was achieved by the wet chemical synthesis, as illustrated in Figure 1. Experimental details are in the supplementary material. The octahedron AgCl microcrystals were first transformed into hexapods shape and then into hexapods with mace pods shape. For the synthesis process, in particular, diallyldimethylammonium chloride (DDA) was used not only as a source of Cl^- but as a stabilizer, which plays a vital role in the morphology control of AgCl crystals. Furthermore, the rate of degradation of methyl orange (MO) by different AgCl morphologies was compared. By controlling the amount of NaBH_4 , we obtained Ag@AgCl microstructure with the different contents of Ag and compared their photocatalytic properties for the degradation of methyl orange (MO).

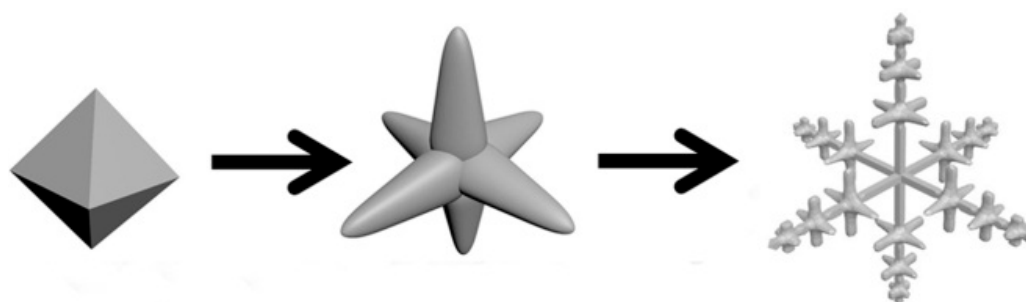


Figure 1. Illustration of silver chloride the shape transformation from octahedra to hexapod with mace pods.

2. Materials and Methods

All reagents and solvents were purchased from commercial sources and used as received without further purification. Chemicals used in this study included silver nitrate (AgNO_3 , A.R. 99.8%, Sinopharm Group Chemical Reagent Co., Ltd., Shanghai, China), nitric acid (HNO_3 , AR) Hydrochloric acid (HCl , AR), diallyldimethylammonium chloride (DDA), ethylene glycol (EG, $\geq 99\%$), sodium borohydride (NaBH_4 , AR, 98%) were purchased from Aladdin. All chemicals were used as received. The solutions were prepared from super pure water (18 $\text{M}\Omega$ cm) purified through a Milli-Q Lab system (Nihon Millipore Ltd., Shanghai, China).

For a typical synthesis of uniform AgCl crystals, 0.8 mL diallyldimethylammonium chloride (DDA) and 20 mL ethylene glycol (EG) were added to a 50 mL flask. The mixture was stirred vigorously

at room temperature for 1 min to mix the DDA and ethylene glycol evenly. Then, 300 μL of 0.1 M AgNO_3 solution were added to the flask. Firstly, we used the oscillator to oscillate 1 min followed with ultrasonic 1 min to make the solution evenly. Then, the solution was placed in a 190 $^\circ\text{C}$ oil bath and reacted with intense agitation. All of the glassware used in the experiments were cleaned in a bath of freshly prepared aqua regia ($\text{HCl}/\text{HNO}_3 = 3:1$) and rinsed thoroughly in deionized water and ethanol. When the reaction was stopped, the flask was placed in an ice bath and quenched. The resulting products were firstly centrifuged at 10,000 r/min for 15 min to remove the supernatant and the products were washed twice with ethanol and water, respectively.

An amount of 100 mg of dried AgCl hexapods with mace pods crystals were weighed and dispersed in 8 mL of water. Reduction was carried out using a 0.02 M NaBH_4 solution. The volume of the reducing agent was adjusted to control the ratio (R) of the amount of the substance of the NaBH_4 to the AgCl sample, thereby the preparation of Ag@AgCl had different degrees of reduction.

The prepared samples were characterized by optical microscopy, X-ray diffraction (XRD) and scanning electron microscope (SEM). The phases of samples were characterized by XRD (Cu $\text{K}\alpha 1$ radiation, Rigaku/Ultima IV, Japan). The morphologies and structures of samples were studied using SEM (3.0 kV, SU70, Hitachi, Japan).

The photo catalytic performance of Ag@AgCl microcrystals was evaluated by the degradation of MO using a 300 W Xe arc lamp with UV cut-off filter as the source of visible light ($\lambda > 400$ nm). Firstly, 50 mg of sample was dispersed in 50 mL of MO solution (10 mg/L) and was stirred for 60 min in the dark to make absorption equilibrium on the surface of the catalysts. Then, the mixed solution was exposed to visible light, and the absorbance was measured by taking a 3 mL of solution every 10 min.

3. Results and Discussion

The SEM images of the AgCl crystals morphologies obtained at different amounts of DDA (from 0.4 mL to 1 mL) are shown in Figure 2. When AgNO_3 was added to the EG solution of the DDA, the solution immediately became milky white and opaque, and then the solution gradually became colourless and transparent as the reaction progressed. We guess that AgCl firstly is formed so the solution becomes milky white and opaque. Then AgCl is dissolved under the effect of DDA and high temperature, thus the solution becomes colourless again. In the reaction system, the concentration of Ag^+ is 1.4×10^{-3} mol/L and $\text{DDA}(\text{Cl}^-)$ is 7.1×10^{-2} mol/L when the volume is 0.4 mL. So we suspect that in a high Cl^- environment the original AgCl ($K_{\text{sp}} = 1.77 \times 10^{-10}$) is transformed into AgCl_2^- ($K_{\text{f}} = 2.5 \times 10^{-5}$) [47,48]. Figure 2 displays the SEM images of AgCl crystals at different amounts of DDA, which shows the gradual transformation of the octahedral into hexapods. The corresponding low magnification images are shown in Supplementary Materials Figures S1–S7 (ESI). From Figure 2a, we can see that under the synergistic effect of EG and DDA, the octahedral AgCl crystals with an edge length of 2 μm are formed after the reaction mixture is refluxed at 190 $^\circ\text{C}$. Previous reports have proven that poly(diallyldimethylammonium) chloride (PDDA) was adsorbed to the {111} facet during the nucleation process of face-centered-cubic (fcc) crystal [49]. Hence, we speculate DDA, which is the monomer of PDDA, also has the effect on leading to the formation of AgCl octahedron. Then, when the amount of DDA increases to 0.5 mL, the size of the octahedron AgCl crystals increases (2.5 μm) and the six corners of octahedron crystals are ‘pulled out’ (Figure 2b). Then AgCl crystals continue to grow along the six corners of the octahedron seeds (Figure 2c) as the amount of DDA reaches 0.7 mL. When the amount of DDA increases to 0.8 mL, the octahedron is completely transformed into hexapods with round pods (Figure 2d).

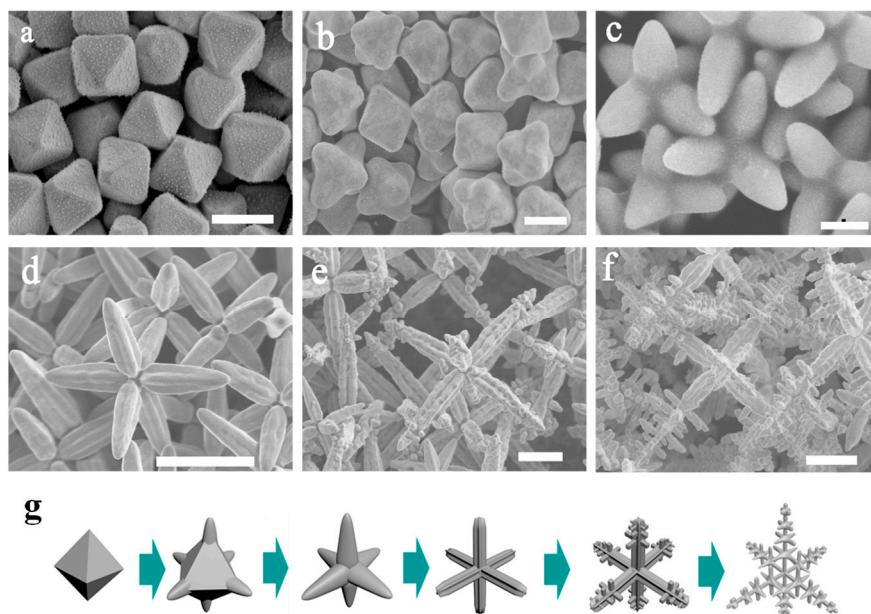


Figure 2. (a–f) SEM images of AgCl microcrystals for different amount of DDA (a) 0.4 mL; (b) 0.5 mL; (c) 0.7 mL; (d) 0.8 mL; (e) 0.9 mL and (f) 1 mL. (g) Illustration of shape transformation of AgCl crystals. Scale bar: 2 μm (a–c); 10 μm (d–f).

As the amount of DDA increases from 0.8 mL to 0.9 mL, the size of hexapods AgCl crystals gradually grows from 3 μm (Figure 2d) to 10 μm (Figure 2e). When the amount of DDA is 0.9 mL, the morphologies of AgCl microcrystals change from hexapods with round pods to regular hexapods with 4-blade arrowhead pods morphologies (Figure 2e), which is the same as in the previous report. Since a rapid growth in $\langle 100 \rangle$ directions along the pod length and the $\{110\}$ growth is suppressed, a groove is formed between adjacent blades on the same pod [46]. With the reaction process ongoing, the growth direction of AgCl crystal changes from $\langle 100 \rangle$ to $\langle 110 \rangle$. From Figure 2e, we can see that the small pods grow out of the triangular groove along the direction of $\langle 110 \rangle$. This step is start at the tip of 4-blade arrowhead pods. When the amount of DDA increases to 1 mL, regular hexapods with mace pods AgCl microcrystals are obtained distinctly (Figure 2f). When we continue to extend the amount of DDA, the morphology of AgCl microcrystals becomes irregular as showed in Figure S8. Figure 2g shows the corresponding shape transformation model of AgCl crystals.

The XRD patterns of the AgCl microcrystals shown in Figure 3a are characterized by the lattice spacing corresponding to the plane families: 111, 200, 220, 311, 222, 400, 331, and 420, which comes out from the fcc crystal lattice of AgCl (JCPDS no. 85–1355). Figure 3A(a–f), shows the XRD patterns of AgCl microcrystal prepared at different DDA amounts (a) 0.4 mL; (b) 0.6 mL; (c) 0.7 mL; (d) 0.8 mL; (e) 0.9 mL; and (f) 1 mL. As shown in Figure 3A, when the peak of $\{200\}$ becomes stronger, the peak of $\{111\}$ becomes weaker as the reaction time increases. Figure 3B shows the formation process of hexapods with mace pods crystals. In conclusion, due to the synergistic effect of both EG and DDA, octahedral AgCl microcrystals are firstly formed. The reactivity of octahedron in different sites is supposed to decrease in the order of corners, edges, and faces [50]. With insufficient supply of Ag^+ , the Ag^+ is preferentially reacted with Cl^- absorbed on corners. When the amount of DDA increases, octahedral AgCl microcrystals grow in the direction of $\langle 100 \rangle$ to form hexapods with round pods crystals. Due to the rapid growth in $\langle 100 \rangle$ directions along the pod length, hexapods with round pods AgCl crystals transform to the regular hexapods with 4-blade arrowhead pods crystals. Eventually, the small pods grow out of the triangular groove in the $\langle 110 \rangle$ direction to form hexapods with mace pods crystals.

Due to the poor absorption of visible light by AgCl, we also studied the photocatalytic properties of Ag@AgCl hexapods with mace pods crystals. AgCl is reduced with various amounts of NaBH_4 at room temperature, thus the Ag@AgCl microstructure is formed. The mole ratio (R) of NaBH_4 to

AgCl is 0.02, 0.05, 0.3, 0.6, and 0.9, respectively, corresponding to different Ag content. Figure S9 shows Ag@AgCl crystals at different R values. It can be found that the surface of AgCl gradually becomes rough and Ag particles appears. When R is gradually increased, the amount of Ag particles increases and even connects into Ag blocks. In order to eliminate possible influencing factors, we conducted a controlled experiment of MO adsorption on the catalyst surface and natural decomposition of MO under visible light in dark conditions. It can be seen from Figure S10 that MO has no significant degradation in 60 min under the above two conditions.

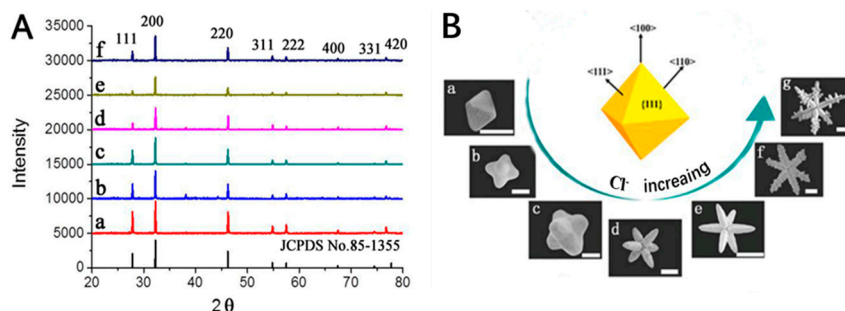


Figure 3. (A) XRD of the as-prepared AgCl microcrystals; (B) Schematic drawing shows facets and growth directions of 3D AgCl microstructures from octahedral seeds. Scale bar: 2 μm (a–d); 10 μm (e–g).

The photo catalytic activity of prepared Ag@AgCl microcrystals were investigated for decomposition of MO induced by visible light ($\lambda > 420 \text{ nm}$) at room temperature [51] (see the details in the ESI). Figure 4A is the absorption spectra, which shows the variation of MO degradation using Ag@AgCl with $R = 0.02$. The absorption peak of MO rapidly decreases and MO is completely degraded at 40 min. The Ag@AgCl microstructure shows an excellent catalytic performance. The absorption spectra of MO degradation using Ag@AgCl microstructures with different Ag content are shown in Figure S11. As the Ag content increases, the degradation rate of MO gradually becomes slower (Figure 4B). When R is greater than 0.05, MO cannot be completely degraded within 60 min. When $R = 0.9$, it is observed that MO only degrades by 20%, indicating that the catalytic performance of Ag@AgCl microstructure has decreased significantly. It can be seen that as the content of silver increases, the catalytic performance of the microstructure gradually weakens. Therefore, the results clearly demonstrate that Ag@AgCl hexapods having a small amount of Ag particles can enhance the photocatalytic activity. Meanwhile, with more Ag particles, the catalytic performance of Ag@AgCl microstructure decreases.

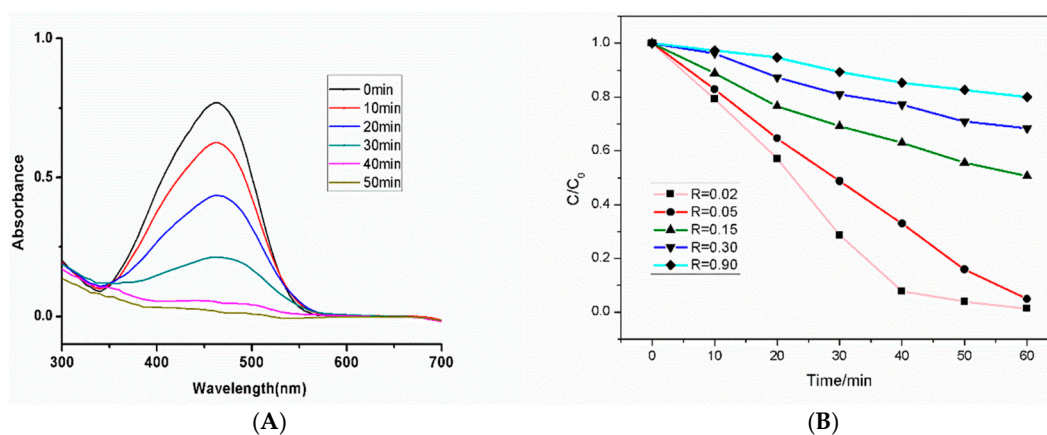


Figure 4. (A) Absorption spectra of the MO at different times with the assistance of the hexapods with mace pods Ag@AgCl microcrystal ($R = 0.02$); (B) Comparison of degradation of MO by Ag@AgCl with different Ag content.

In order to truly determine the relationship between silver content and catalytic performance, EDS spectra are used to determine the content of Ag and AgCl. The EDS elemental mapping images of Ag@AgCl in Figure 5B,C clearly illustrate the distribution of Ag and Cl. As shown in Figure 5D, when R reaches 0.9, the content of Ag reaches 99.61% (wt %), and only a small amount of Cl (0.39%) remains, suggesting that almost all of AgCl is reduced, and the surface of the structure is covered by the Ag blocks. At this time, the photocatalytic performance of the Ag@AgCl microstructure is theoretically weak, which is consistent with the photocatalytic results obtained in Figure 4B. The EDS mapping images of low Ag content are shown in Figure S12. The weight proportion of Ag is 83.65%, indicating the presence of a small amount of Ag particles. It is consistent with its better catalytic results.

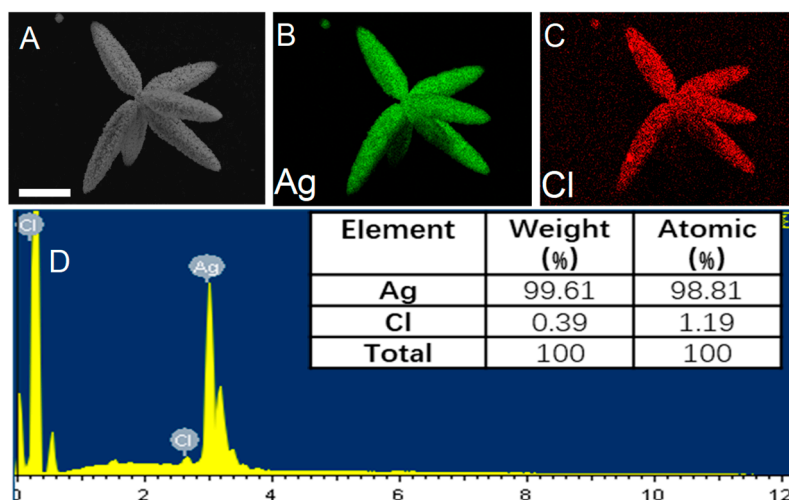


Figure 5. (A) SEM image of Ag@AgCl microstructure ($R = 0.9$); (B) and (C) EDS elemental mapping of Ag@AgCl indicating the Ag and Cl elemental distribution. (D) The corresponding EDS elemental spectrum of Ag@AgCl microstructure. Scar bar: $8 \mu\text{m}$ (A–C).

In the process of degradation, when there are separated Ag nanoparticles on the surface, photoinduced electrons are easily transferred to the Ag surface due to the presence of SPR, which improves the efficiency of separation from electron holes. Photoelectrons are trapped by O_2 in the solution to produce active substances such as superoxide ions, so the photocatalytic performance is greatly improved [51]. In the meantime, the holes are transferred to the surface of AgCl due to the high oxidation ability of the chloride ions is presented in AgCl. These leads to the oxidation of Cl^- ions to form Cl^0 atoms. As chlorine atoms are reactive radical species, they should be able to oxidize MO dye, which is reduced to chloride ions again at the same time [52]. Therefore, the synergistic effect between Ag and AgCl promotes the degradation of MO as described above. When there is a small amount of Ag particles on the Ag@AgCl surface ($R = 0.02, 0.05$), the degradation rate is fast. However, with the increasing of Ag content, we suspect that the reduction of AgCl leads to a decline in catalytic performance. When the degree of reduction is increased in Ag@AgCl ($R = 0.15, 0.3, 0.9$), the number of Ag particles on the surface is greatly increased and connects into a block. Also, AgCl is greatly reduced. As a result, Cl^- adsorbed on AgCl is greatly reduced as well. Then Cl^0 almost no longer produced, and the synergy greatly weakened. Thus, the photocatalytic effect of Ag@AgCl microstructure is greatly reduced.

4. Conclusions

In conclusion, for the first time, AgCl hexapods with mace pods crystals are synthesized by one-pot synthesis method, and the stepwise evolution of octahedral AgCl microcrystals into hexapods with mace pods crystals is observed. The octahedral AgCl microcrystals are firstly grown along the direction of $\langle 100 \rangle$ to form hexapods with 4-blade arrowhead pods crystals. Then, hexapods with 4-blade arrowhead pods AgCl crystals are transformed with regard to the growth direction from $\langle 100 \rangle$

to $\langle 110 \rangle$, and eventually form hexapods with mace pods crystals. Moreover, by regulating the mole ratio of NaBH_4 to AgCl , we find that when $R = 0.02$, the microstructure has a high catalytic effect. This work not only provides a method to prepare different morphology AgCl microcrystals, but also provides new insights into the crystal growth habit.

Supplementary Materials: The following are available online at <http://www.mdpi.com/2073-4352/9/8/401/s1>, Figure S1: SEM image of AgCl microcrystals at 0.4 mL DDA. Left: High magnification, Right: Low magnification; Figure S2: SEM images of AgCl microcrystals at 0.5 mL DDA. Left: High magnification, Right: Low magnification; Figure S3: SEM images of AgCl microcrystals at 0.6 mL DDA. Left: High magnification, Right: Low magnification; Figure S4: SEM images of AgCl microcrystals at 0.7 mL DDA. Left: High magnification, Right: Low magnification; Figure S5: SEM images of AgCl microcrystals at 0.8 mL DDA. Left: High magnification, Right: Low magnification; Figure S6: SEM images of AgCl microcrystals at 0.9 mL DDA. Left: High magnification, Right: Low magnification; Figure S7: SEM images of AgCl microcrystals at 1 mL DDA. Left: High magnification, Right: Low magnification; Figure S8: SEM images of AgCl microcrystals at high amount of DDA. Figure S9: SEM images of Ag@AgCl with different content of Ag , $R = 0.05, 0.15, 0.3, 0.9$. Left: Low magnification, Right: High magnification; Figure S10: The absorption spectra of photocatalytic MO degradation of Ag@AgCl with different conditions: (A) no catalyst under visible light (B) with catalyst in the dark. (C) Comparison of degradation of MO with time under the two conditions above; Figure S11: The absorption spectra of photocatalytic MO degradation of Ag@AgCl with different degrees of reduction: (A) $R = 0.05$ (B) $R = 0.15$ (C) $R_n = 0.3$ (D) $R = 0.9$; Figure S12: EDS elemental mapping of Ag@AgCl ($R = 0.15$) indicating the Ag and Cl elemental distribution and the corresponding EDS elemental spectrum of Ag@AgCl microstructure. Scar bar: $4 \mu\text{m}$; Figure S13: EDS elemental mapping of Ag@AgCl ($R = 0.6$) indicating the Ag and Cl elemental distribution and the corresponding EDS elemental spectrum of Ag@AgCl microstructure. Scar bar: $4 \mu\text{m}$.

Author Contributions: Conceptualization, Y.L. and Y.Q.; methodology, Y.L.; validation, Y.Q. and J.Z.; resources, J.Z.; data curation, D.Y.; writing—original draft preparation, Y.L.; writing—review and editing, Y.Q.; visualization, D.Y.; supervision, Y.L.; project administration, J.Z.

Funding: This work was supported by the National Key R&D Program of China (2016YFC0800902) and the Key R&D Program Projects of Zhejiang Province (2018C03G2011156).

Conflicts of Interest: The authors declare no conflict of interest.

References

1. Leonardi, A.; Engel, M. Particle Shape Control via Etching of Core@Shell Nanocrystals. *ACS Nano* **2018**, *12*, 9186–9195. [[CrossRef](#)] [[PubMed](#)]
2. Qin, Y.Z.; Pan, W.F.; Yu, D.D.; Lu, Y.X.; Wu, W.H.; Zhou, J.G. Stepwise evolution of Au micro/nanocrystals from an octahedron into a truncated ditetragonal prism. *Chem. Commun.* **2018**, *54*, 3411–3414. [[CrossRef](#)]
3. Satyavolu, N.S.R.; Tan, L.H.; Lu, Y. DNA-Mediated Morphological Control of Pd–Au Bimetallic Nanoparticles. *J. Am. Chem. Soc.* **2016**, *138*, 16542–16548. [[CrossRef](#)]
4. Liu, P.; Qin, R.; Fu, G.; Zheng, N. Surface Coordination Chemistry of Metal Nanomaterials. *J. Am. Chem. Soc.* **2017**, *139*, 2122–2131. [[CrossRef](#)] [[PubMed](#)]
5. Zhang, J.; Zhang, P.; Wang, T.; Gong, J. Monoclinic WO_3 nanomultilayers with preferentially exposed (002) facets for photoelectrochemical waters plitting. *Nano Energy* **2015**, *11*, 189–195. [[CrossRef](#)]
6. Zheng, Y.Q.; Ma, Y.Y.; Zeng, J.; Zhong, X.L.; Jin, M.S.; Li, Z.Y.; Xia, Y.N. Seed-Mediated Synthesis of Single-Crystal Gold Nanospheres with Controlled Diameters in the Range 5–30 nm and their Self-Assembly upon Dilution. *Chem. Asian J.* **2013**, *8*, 792–799. [[CrossRef](#)]
7. Zheng, Y.Q.; Zhong, X.L.; Li, Z.Y.; Xia, Y.N. Successive, Seed-Mediated Growth for the Synthesis of Single-Crystal Gold Nanospheres with Uniform Diameters Controlled in the Range of 5–150 nm. *Part. Part. Syst. Charact.* **2013**, *31*, 266–273. [[CrossRef](#)]
8. Ruditskiy, A.; Xia, Y.N. Toward the Synthesis of Sub-15 nm Ag Nanocubes with Sharp Corners and Edges: The Roles of Heterogeneous Nucleation and Surface Capping. *J. Am. Chem. Soc.* **2016**, *138*, 3161–3167. [[CrossRef](#)]
9. Zhou, S.; Li, J.H.; Gilroy, K.D.; Tao, J.; Zhu, C.L.; Yang, X.; Sun, X.J.; Xia, Y.N. Facile Synthesis of Silver Nanocubes with Sharp Corners and Edges in an Aqueous Solution. *ACS Nano* **2016**, *10*, 9861–9870. [[CrossRef](#)] [[PubMed](#)]
10. Xiong, Y.J.; Chen, J.; Wiley, B.; Xia, Y.N.; Yin, Y.D.; Li, Z.Y. Size-Dependence of Surface Plasmon Resonance and Oxidation for Pd Nanocubes Synthesized via a Seed Etching Process. *Nano Lett.* **2005**, *5*, 1237–1242. [[CrossRef](#)]

11. Liu, H.P.; Zhong, P.; Liu, K.; Han, L.; Zheng, H.Q.; Yin, Y.D.; Gao, C.B. Synthesis of ultrathin platinum nanoplates for enhanced oxygen reduction activity. *Chem. Sci.* **2018**, *9*, 398–404. [[CrossRef](#)]
12. Yin, X.; Shi, M.; Kwok, K.S.; Zhao, H.D.; Gray, D.L.; Bertke, J.A.; Yang, H. Dish-like higher-ordered palladium nanostructures through metal ion-ligand complexation. *Nano Res.* **2018**, *11*, 3442–3452. [[CrossRef](#)]
13. Zeng, J.; Xia, X.H.; Rycenga, M.; Henneghan, P.; Li, Q.G.; Xia, Y.N. Successive Deposition of Silver on Silver Nanoplates: Lateral versus Vertical Growth. *Angew. Chem.* **2011**, *123*, 258–263. [[CrossRef](#)]
14. Rubio, G.G.; Oliveira, T.M.; Altantzis, T.; Porta, A.L.; Guerrero-Martínez, A.; Bals, S.; Scarabelli, L.; Marzan, L.M.L. Disentangling the effect of seed size and crystal habit on gold nanoparticle seeded growth. *Chem. Commun.* **2017**, *53*, 11360–11363. [[CrossRef](#)]
15. Ge, Y.J.; Duan, X.D.; Zhang, M.; Mei, L.; Hu, J.W.; Hu, W.; Duan, X.F. Direct Room Temperature Welding and Chemical Protection of Silver Nanowire Thin Films for High Performance Transparent Conductors. *J. Am. Chem. Soc.* **2018**, *140*, 193–199. [[CrossRef](#)]
16. Yang, Y.; Wang, W.F.; Li, X.L.; Chen, W.; Fan, N.N.; Zou, C.; Chen, X.; Xu, X.J.; Zhang, L.J.; Huang, S.M. Controlled Growth of Ag/Au Bimetallic Nanorods through Kinetics Control. *Chem. Mater.* **2013**, *25*, 34–41. [[CrossRef](#)]
17. Lee, S.; Bae, C.; Lee, J.; Lee, S.; Oh, S.H.; Kim, J.Y.; Park, G.S.; Jung, H.S.; Shin, H. Fabrication of a Stable New Polymorph Gold Nanowire with Sixfold Rotational Symmetry. *Adv. Mater.* **2018**, *30*, 1706261. [[CrossRef](#)]
18. Rubio, G.G.; Núñez, P.D.; Rivera, A.; Prada, A.; Tardajos, G.; Izquierdo, J.G.; Bañares, L.; Llombart, P.; Macdowell, L.G.; Palafox, M.A.; et al. Femtosecond laser reshaping yields gold nanorods with ultranarrow surface plasmon resonances. *Science* **2017**, *358*, 640–644. [[CrossRef](#)]
19. Xie, J.; Zhang, Q.; Lee, J.Y.; Wang, D.I.C. The Synthesis of SERS-Active Gold Nanoflower Tags for In Vivo Applications. *ACS Nano* **2008**, *2*, 2473–2480. [[CrossRef](#)]
20. Song, C.Y.; Zhou, N.; Yang, B.Y.; Yang, Y.J.; Wang, L.H. Facile synthesis of hydrangea flower-like hierarchical gold nanostructures with tunable surface topographies for single-particle surface enhanced Raman scattering. *Nanoscale* **2015**, *7*, 17004–17011. [[CrossRef](#)]
21. Martinez, A.G.; Barbosa, S.; Santos, I.P.; Marzan, L.M.L. Nanostars shine bright for you Colloidal synthesis, properties and applications of branched metallic nanoparticles. *Curr. Opin. Colloid Interface Sci.* **2011**, *16*, 118–127.
22. Cheong, S.; Watt, J.; Ingham, B.; Toney, M.F.; Tilley, R.D. In Situ and Ex Situ Studies of Platinum Nanocrystals: Growth and Evolution in Solution. *J. Am. Chem. Soc.* **2009**, *131*, 14590–14595. [[CrossRef](#)]
23. Mulvihill, M.J.; Ling, X.Y.; Henzie, J.; Yang, P. Anisotropic Etching of Silver Nanoparticles for Plasmonic Structures Capable of Single-Particle SERS. *J. Am. Chem. Soc.* **2009**, *132*, 268–274. [[CrossRef](#)]
24. Maksimuk, S.; Teng, X.; Yang, H. Roles of Twin Defects in the Formation of Platinum Multipod Nanocrystals. *J. Phys. Chem. C* **2007**, *111*, 14312–14319. [[CrossRef](#)]
25. Yu, T.; Kim, D.Y.; Zhang, H.; Xia, Y. Platinum Concave Nanocubes with High-Index Facets and Their Enhanced Activity for Oxygen Reduction Reaction. *Angew. Chem. Int. Ed.* **2011**, *50*, 2773–2777. [[CrossRef](#)]
26. Jin, M.; Zhang, H.; Xie, Z.; Xia, Y. Palladium Concave Nanocubes with High-Index Facets and Their Enhanced Catalytic Properties. *Angew. Chem. Int. Ed.* **2011**, *50*, 7850–7854. [[CrossRef](#)]
27. Chen, J.; Herricks, T.; Xia, Y. Polyol Synthesis of Platinum Nanostructures: Control of Morphology through the Manipulation of Reduction Kinetics. *Angew. Chem. Int. Ed.* **2005**, *117*, 2645–2648. [[CrossRef](#)]
28. Zhang, H.; Lu, Y.G.; Liu, H.; Fang, J.Z. One-pot synthesis of high-index faceted AgCl nanocrystals with trapezohedral, concave hexoctahedral structures and their photocatalytic activity. *Nanoscale* **2015**, *7*, 11591–11601. [[CrossRef](#)]
29. Dong, R.; Tian, B.; Zeng, C.; Li, T.; Wang, T.; Zhang, J. Ecofriendly Synthesis and Photocatalytic Activity of Uniform Cubic Ag@AgCl Plasmonic Photocatalyst. *J. Phys. Chem. C* **2012**, *117*, 213–220. [[CrossRef](#)]
30. Cheng, L.; Ma, C.; Yang, G.; You, H.; Fang, J. Hierarchical silver mesoparticles with tunable surface topographies for highly sensitive surface enhanced Raman spectroscopy. *J. Mater. Chem. A* **2014**, *2*, 4534–4542. [[CrossRef](#)]
31. Zhang, Q.; Ge, J.; Pham, T.; Goebel, J.; Hu, Y.; Lu, Z.; Yin, Y. Reconstruction of Silver Nanoplates by UV Irradiation: Tailored Optical Properties and Enhanced Stability. *Angew. Chem. Int. Ed.* **2009**, *48*, 3516–3519. [[CrossRef](#)]

32. Wang, P.; Huang, B.B.; Lou, Z.Z.; Zhang, X.Y.; Qin, X.Y.; Dai, Y.; Zheng, Z.K.; Wang, X.N. Synthesis of Highly Efficient Ag@AgCl Plasmonic Photocatalysts with Various Structures. *Chem. Eur. J.* **2010**, *16*, 538–544. [[CrossRef](#)]
33. Zhu, M.; Chen, P.; Liu, M. High-Performance Visible-Light-Driven Plasmonic Photocatalysts Ag/AgCl with Controlled Size and Shape Using Graphene Oxide as Capping Agent and Catalyst Promoter. *Langmuir* **2013**, *29*, 9259–9268. [[CrossRef](#)]
34. Kimijima, K.I.; Sugimoto, T. Growth Mechanism of AgCl Nanoparticles in a Reverse Micelle System. *J. Phys. Chem. B* **2004**, *108*, 3735–3738. [[CrossRef](#)]
35. Lou, Z.; Huang, B.; Wang, Z.; Qin, X.; Zhang, X.; Liu, Y.; Zhang, R.; Dai, Y.; Whangbo, M.-H. Interface kinetic diffusion reaction leading to fast and continuous generation of AgCl nanocubes in NaCl solution. *Dalton Trans.* **2013**, *42*, 15219–15225. [[CrossRef](#)]
36. An, C.; Peng, S.; Sun, Y. Facile Synthesis of Sunlight-Driven AgCl:Ag Plasmonic Nanophotocatalyst. *Adv. Mater.* **2010**, *22*, 2570–2574. [[CrossRef](#)]
37. Tang, Y.; Jiang, Z.; Xing, G.; Li, A.; Kanhere, P.D.; Zhang, Y.; Sum, T.C.; Li, S.; Chen, X.; Dong, Z.; et al. Efficient Ag@AgCl Cubic Cage Photocatalysts Profit from Ultrafast Plasmon-Induced Electron Transfer Processes. *Adv. Funct. Mater.* **2013**, *23*, 2932–2940. [[CrossRef](#)]
38. Han, S.H.; Liu, H.M.; Sun, C.C.; Jin, P.J.; Chen, Y. Photocatalytic performance of AgCl@Ag core-shell nanocubes for the hexavalent chromium reduction. *J. Mater. Sci.* **2018**, *53*, 12030–12039. [[CrossRef](#)]
39. Guo, X.Y.; Deng, D.; Tian, Q.H. One pot controllable synthesis of AgCl nanocrystals with different morphology and their photocatalytic activity. *Powder Technol.* **2017**, *308*, 206–213. [[CrossRef](#)]
40. Ao, Y.H.; Bao, J.Q.; Wang, P.F.; Wang, C. A novel heterostructured plasmonic photocatalyst with high photocatalytic activity: Ag@AgCl nanoparticles modified titanium phosphate nanoplates. *J. Alloy. Comp.* **2017**, *698*, 410–419. [[CrossRef](#)]
41. Bi, Y.P.; Ye, J.H. In situ oxidation synthesis of Ag/AgCl core-shell nanowires and their photocatalytic properties. *Chem. Commun.* **2009**, 6551–6553. [[CrossRef](#)]
42. Bi, Y.P.; Ye, J.H. Heteroepitaxial growth of platinum nanocrystals on AgCl nanotubes via galvanic replacement reaction. *Chem. Commun.* **2010**, *46*, 1532–1534. [[CrossRef](#)]
43. Hu, H.Y.; Jiao, Z.B.; Lu, G.X.; Ye, J.H.; Bi, Y.P. Enhanced photocatalytic properties of biomimetic Ag/AgCl heterostructures. *RSC Adv.* **2014**, *4*, 31795–31798. [[CrossRef](#)]
44. Lou, Z.; Huang, B.; Qin, X.; Zhang, X.; Cheng, H.; Liu, Y.; Wang, S.; Wang, J.; Dai, Y. One-step synthesis of AgCl concave cubes by preferential overgrowth along <111> and <110> directions. *Chem. Commun.* **2012**, *48*, 3488–3490. [[CrossRef](#)]
45. Lou, Z.; Huang, B.; Ma, X.; Zhang, X.; Qin, X.; Wang, Z.; Dai, Y.; Liu, Y. A 3D AgCl Hierarchical Superstructure Synthesized by a Wet Chemical Oxidation Method. *Chem. Eur. J.* **2012**, *18*, 16090–16096. [[CrossRef](#)]
46. Gatemala, H.; Thammacharoen, C.; Ekgasit, S. 3D AgCl microstructures selectively fabricated via Cl⁻ induced precipitation from [Ag(NH₃)₂]⁺. *CrystEngComm* **2014**, *16*, 6688–6696. [[CrossRef](#)]
47. Gatemala, H.; Ekgasit, S.; Pienpinijtham, P. 3D structure-preserving galvanic replacement to create hollow Au microstructures. *CrystEngComm* **2017**, *19*, 3808–3816. [[CrossRef](#)]
48. Abeyweera, S.C.; Rasamani, K.D.; Sun, Y. Ternary Silver Halide Nanocrystals. *Acc. Chem. Res.* **2017**, *50*, 1754–1761. [[CrossRef](#)]
49. Shuford, K.L.; Chen, M.; Lee, E.J.; Cho, S.O. A Facile Polyol Route to Uniform Gold Octahedra with Tailorable Size and Their Optical Properties. *ACS Nano* **2008**, *2*, 1760–1769.
50. Li, C.; He, G.; Jin, M.; Zhang, H.; Lu, N.; Wang, J.; Kim, M.J.; Xia, Y. A Mechanistic Study on the Nucleation and Growth of Au on Pd Seeds with a Cubic or Octahedral Shape. *ChemCatChem* **2012**, *4*, 1668–1674.
51. Wang, P.; Huang, B.; Qin, X.; Zhang, X.; Dai, Y.; Wei, J.; Whangbo, M. Ag@AgCl: A Highly Efficient and Stable Photocatalyst Active under Visible Light. *Angew. Chem. Int. Ed.* **2008**, *47*, 7931. [[CrossRef](#)]
52. Devi, T.B.; Begum, S.; Ahmaruzzaman, M. Photo-catalytic activity of Plasmonic Ag@AgCl nanoparticles (synthesized via a green route) for the effective degradation of Victoria Blue B from aqueous phase. *J. Photochem. Photobiol. B Biol.* **2016**, *160*, 260–270. [[CrossRef](#)]

